PAPER

Bowing of the band gap and spin-orbit splitting energy in BGaAs

Materials Research Express

PAPER

Bowing of the band gap and spin-orbit splitting energy in BGaAs

RECEIVED
8 October 2019

REVISED
28 November 2019

ACCEPTED FOR PUBLICATION
17 December 2019

PUBLISHED
8 January 2020

R Kudrawiec[1,4], M P Polak[1,4], K M McNicholas[2], J Kopaczek[1], M A Wistey[3] and S R Bank[2]

[1] Faculty of Fundamental Problems of Technology, Wroclaw University of Science and Technology, Wybrzeze Wyspianskiego 27, Wroclaw, 50-370, Poland
[2] Microelectronics Research Center, University of Texas at Austin, Austin, TX 78758, United States of America
[3] Department of Physics, Texas State University, 601 University Drive, San Marcos, Texas, 78666, United States of America
[4] R Kudrawiec and M P Polak contributed equally to this work.

E-mail: robert.kudrawiec@pwr.edu.pl

Keywords: BGaAs, band gap bowing, spin-orbit splitting, photoreflectance, DFT calculations

Abstract

BGaAs layers with the boron concentration up to 17.7% have been grown by molecular beam epitaxy on GaAs and GaP substrates and studied by photoreflectance (PR) spectroscopy. The direct optical transitions between the valence band (heavy hole, light hole, and the spin–orbit split-off band) and the conduction band have been observed in PR spectra. The bowing parameter for the band gap and the spin–orbit splitting has been determined from PR studies to be 3.6 $\pm$ 0.2 and 0.2 $\pm$ 0.1 eV, respectively. These values are very close to those determined using state-of-the-art first principle density functional methods (b_{dir} = 3.5 $\pm$ 0.1 eV and b_{SO} = 0.06 $\pm$ 0.02 eV). In addition, the indirect band gap has been examined theoretically and the bowing parameter has been determined to be 2.3 $\pm$ 0. eV, with the crossing between the direct and indirect gap in BGaAs at ~12% B.

1. Introduction

III-V alloys containing boron remain some of the least explored III-V compound semiconductors. Of these alloys, BGaAs has been studied most intensively in recent years; however challenging synthesis has limited the achievable boron concentration regime to <5%–8% [1–10]. A reduction of the BGaAs lattice constant with increasing B concentration is well documented experimentally [1, 4, 10], but the effects of B incorporation on the band gap have been less explored. According to theoretical calculations [11–13] the boron related changes in the band gap are negligible when the boron concentration is below ~5% because of large band gap bowing (b = 3.5 eV) [11]. At these dilute concentrations, boron containing alloys have potential applications for strain compensation in long-wavelength GaInAs/GaAs quantum wells (QWs), motivating experimental exploration of the band gap of such alloys. To date, BGaAs films with dilute boron concentrations have typically been grown on GaAs substrates. In such samples the optical signal from BGaAs (photoluminescence or the absorption edge) is obscured by the signal from the GaAs template/substrate, making experimental observations of the electronic band structure challenging. As a result, the effects of boron incorporation on the band gap of BGaAs remain insufficiently analyzed. Moreover, the influence of boron on the spin–orbit splitting has not been studied experimentally.

Synthesis of high-quality BGaAs with higher boron concentrations (B > 5%–8%) has proven more challenging, with no reports of concentrations exceeding 8%. As shown in figure 1(a), BGaAs would be lattice-matched to GaP at B = 23%, making BGaAs layers with boron concentration >5% very interesting for BGaAs/GaP QWs since such structures can be epitaxially integrated with a Si platform via well-developed GaP/Si templates. This possibility further motivates the characterization of electronic band structure of BGaAs alloys outside the dilute regime with precise characterization techniques such as photoreflectance (PR).

To date, PR investigations of the electronic structure of BGaAs alloys have been extremely limited [3]. The high-sensitivity resulting the differential-like nature of the PR technique make it an excellent tool to study the direct optical transitions in semiconductor alloys. This technique has been widely applied to study the electronic band structure of highly mismatched alloys [15–17], i.e. alloys similar to BGaAs because of the large differences in the electronegativity and size of B and Ga atoms. In this work we report very systematic PR studies of the band

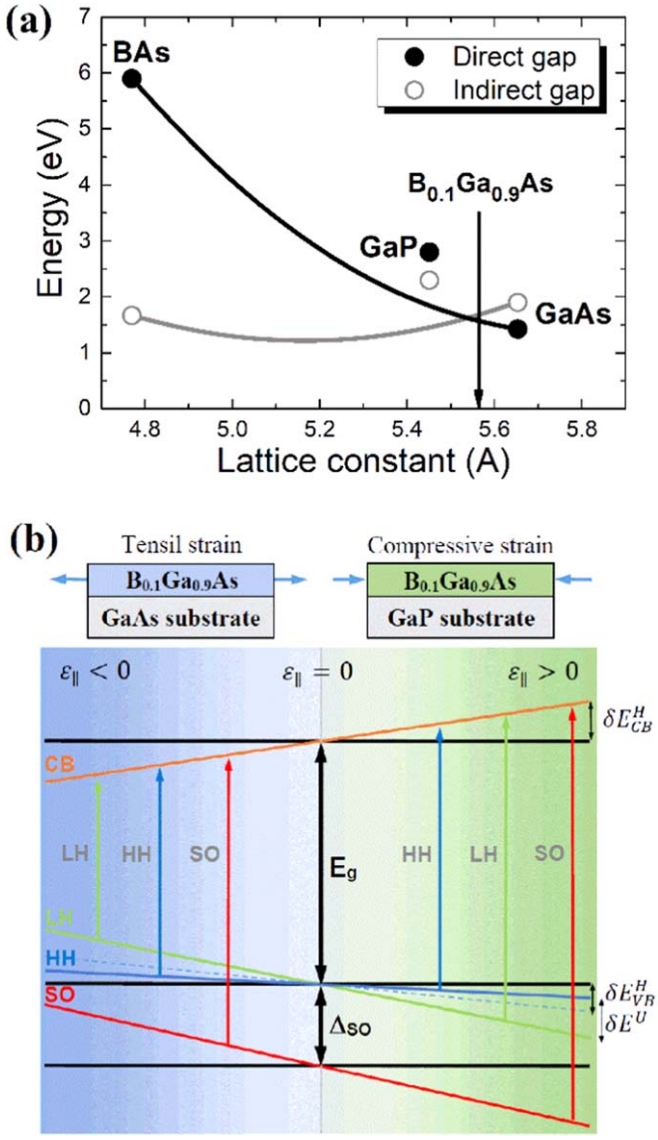

Figure 1. (a) Band gap versus the lattice constant in BGaAs. Values of band gaps and the lattice constants for III-V compounds are taken from [14]. (b) The influence of the tensile and compressive strain on direct optical transitions at the Γ point of Brillouin zone in $B_{0.1}Ga_{0.9}As$ layer grown on GaAs and GaP substrate, respectively.

gap and the spin–orbit splitting for BGaAs layers with boron concentration up to 17.7%. The direct optical transitions between the valence band and the conduction band have been clearly observed and carefully analyzed. The bowing parameter of the band gap and the spin–orbit splitting has been determined experimentally and compared with the bowing parameter obtained from theoretical calculations performed with state-of-the-art density functional theory (DFT) methods.

2. Experimental and theoretical details

BGaAs layers were grown by solid-source molecular beam epitaxy (MBE) on GaAs and GaP substrates using an EPI Mod Gen II MBE system. The BGaAs samples were grown at ~1.8–2.0 Å sec^{-1}, with a Ga flux of 3.98×10^{14} atoms/(cm^2 sec.), corresponding to a Ga beam equivalent pressure (BEP) of 1.67×10^{-7}Torr. Boron deposition was performed using an electron beam evaporator. Eutectic reactions between the beam flux ionization gauge filaments and elemental B prohibit direct measurement of the B BEP. Instead, the B fluxes were calibrated using x-ray diffraction to measure the boron concentration as a function of evaporator power in a series of BGaAs calibration growths. The As_2:Ga flux ratio was 4.4, corresponding to a Ga:As BEP ratio of ~18 for all BGaAs growths. The substrate temperature was monitored using optical pyrometry and was maintained at 400 C during the growth of the BGaAs layers. Additionally, a Bi overpressure of 5×10^{-8}Torr, corresponding to a surface coverage of ~1.4% was supplied to act as a surfactant and promote substitutional incorporation of B.

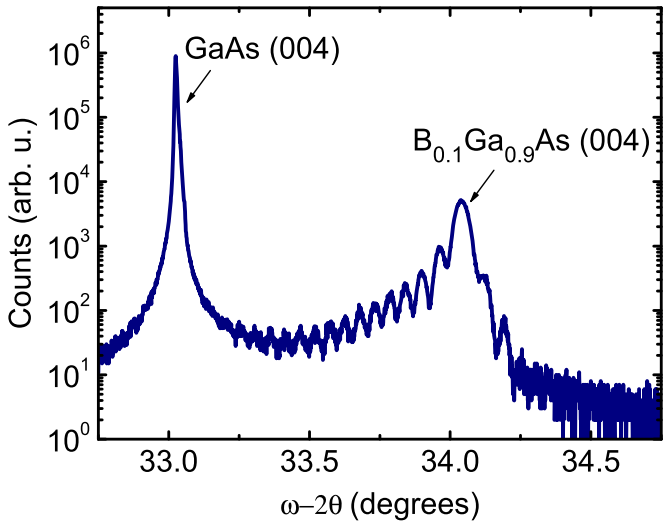

Figure 2 High-resolution x-ray diffraction $\omega-2\theta$ data from a 100 nm thick $B_{0.1}Ga_{0.9}As$ layer on GaAs.

High-resolution x-ray diffraction $\omega-2\theta$ measurements about the GaAs (004) diffraction peak were performed with a Rigaku SmartLab diffractometer in order to determine the lattice parameters, crystal quality, and boron concentration in all samples. The boron concentrations were calculated from the measured lattice constants by linearly interpolating between the lattice constants of BAs and GaAs, assuming 100% substitutional B incorporation. Strain induced deformation of the BGaAs lattice was accounted for in coherent samples by linearly interpolation of the elastic constants predicted from first principles calculations for BAs, as described below, and standard values from the International Crystal Structure Database for GaAs. Characteristic x-ray diffraction $\omega-2\theta$ data from a 100 nm thick $B_{0.1}Ga_{0.9}As/GaAs$ sample is shown in figure 2.

PR spectra were measured with a 'bright configuration' of experimental set-up [14] equipped with a single grating 0.5 meter focal-length monochromator, a Si *pin* photodiode, a 150 W tungsten-halogen lamp as the probing source and a continuous wave laser (405 nm line) as the pump source. The pump beam was modulated by a mechanical chopper at a frequency of 280 Hz. Phase sensitive detection of the PR signal was accomplished using a lock-in amplifier.

The DFT calculations [18, 19] were performed on 128 atom supercells (a 4 $\times$ 4x4 multiplication of the primitive 2 atom unit cell), with the use of the VASP package [20, 21] and PAW potentials [22]. The B and As atoms were distributed within the supercell according to special quasirandom structures (SQS) [23], which were generated individually for each composition using the mcsqs code [24], where pairs, triplets, and quadruplets were taken into account for three, two and two nearest-neighbors respectively. The Monte Carlo procedure was carried out until either the objective function converged or a perfect match was found. This allowed to study 64 boron compositions in 1.56% intervals. Full geometry optimization (internal ionic degrees of freedom and lattice constants) was performed for all compositions using the PBEsol functional best suited for lattice properties of semiconductors [25], where the forces acting on an individual atom were converged down to not exceed 0.001 eV $Å^{-1}$. Then the optimized geometry was used in the electronic band structure calculations with the modified Becke-Johnson (mBJ) functional [26], which was proven to have an accuracy in determining the band gap comparable with hybrid functionals while keeping the computational efficiency of meta-GGA functionals [27, 28]. All calculations were performed using 2x2x2 Monkhorst-Pack k-point mesh [29] with spin–orbit interaction included. The experimental knowledge of the electronic band structure of the highly-explored GaAs allowed us to use the 'c' parameter in the mBJ functional (equation (3) in [26]) to slightly adjust the calculated band gap in order to perfectly reproduce the experimental value which provided a solid starting point for the calculations. Pure BAs however, has not been experimentally studied in detail before. In lieu of this, we used self-consistent calculations to determine the 'c' parameter for BAs. Linear interpolations between the two binary parameters were used to calculate the 'c' parameters for the BGaAs alloys, an approach commonly used in previous studies of similar systems [30, 31]. Due to the indirect character of BAs as well as the large boron concentrations in these alloys, the band structures of supercells obstructed by folding of the bands inside the smaller Brillouin zone were unfolded using the spectral weight approach [32, 33], with the use of the fold2bloch code [34].

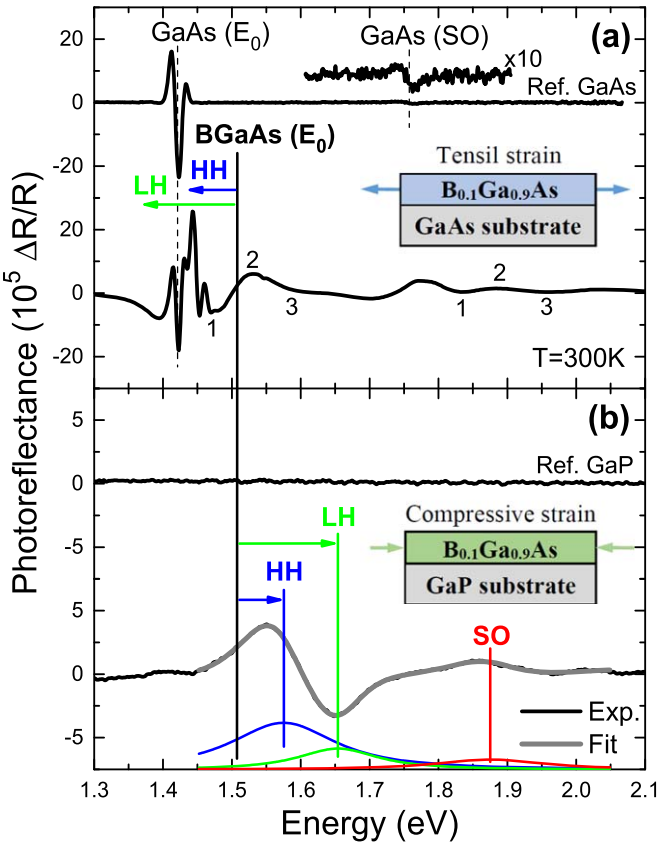

Figure 3 (a) Room temperature photoreflectance spectra of reference GaAs and $B_{0.1}Ga_{0.9}As$ layer grown on GaAs (a) and reference GaP and $B_{0.102}Ga_{0.898}As$ layer grown on GaP (b).

3. Results and discussion

Figures 3(a) and (b) show a comparison of PR spectra measured from BGaAs layers with ~10% B grown on GaAs and GaP substrate, respectively. For reference, PR spectra measured form bare GaAs and GaP substrates are also shown. As shown in figure 3(a), the direct optical transitions between the valence band and the conduction band in the BGaAs layer interferes with the direct optical transitions in the underlying GaAs substrate. The spectral overlap of these features makes direct determination of the band gap and the spin–orbit splitting in BGaAs layers grown on GaAs difficult. Additionally, the built-in electric field results in Franz-Keldysh oscillations (FKOs), further complicating analysis of the measured PR spectra on GaAs substrates. We attribute the presence of the electric field in these samples to different Fermi level pinning/location at BGaAs surface and BGaAs/GaAs interface, as well as unintentional doping. An example of Te doped BGaAs layers grown on GaAs, where the BGaAs PR signal is easily recognizable, is shown in figure 4. For these samples the narrow PR resonance at 1.42 eV is associated with the optical transition in GaAs buffer layer and the broad PR resonance followed by FKO is related to the band-to-band absorption in Te doped BGaAs layer. Due to the Fermi level pinning at a characteristic energy at BGaAs surface, a surface depletion layer with a strong built-in electric field is present in BGaAs layers (see sketch in figure 4) and thereby FKO is observed for these samples. The presence of FKO present a distinct PR signal originating from the BGaAs epilayers. However, detailed analysis of the FKO spectral feature in these samples is complicated by strain-induced splitting of the valence bands, as shown schematically in figure 1(b).

For BGaAs layers grown on GaP substrates, BGaAs-related transitions do not interfere with GaP-related transitions since no optical transitions are present for GaP in this spectral range; see the reference sample in figure 3(b). Because of this, BGaAs layers grown on GaP substrates present an excellent opportunity to study the direct optical transitions and gap bowing in BGaAs alloys. A strong built-in electric field is not present in these samples and therefore energies of these transitions can be analyzed using Aspnes' formula [35]:

$$\frac{\Delta R}{R}(E) = \sum_{n}^{j=1} [C_j e^{i\theta_j}(E - E_j + i\Gamma_j)^{-m_j}], \quad (1)$$

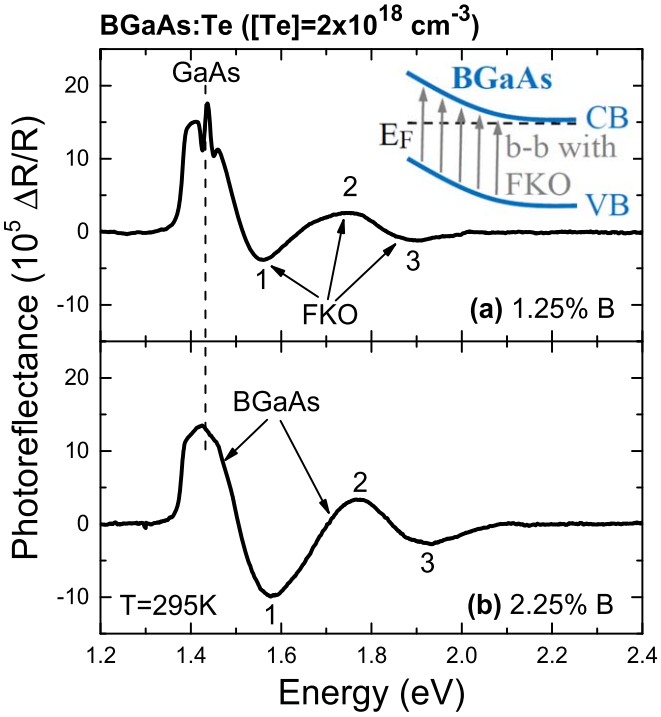

Figure 4 Room temperature photoreflectance spectra of Te-doped BGaAs layer with 1.25%B (a) and 2.25% B (b) grown on GaAs substrate. The inset sketch shows the band-to-band (b-b) transition in the samples with strong built-in electric field which is responsible for Franz-Keldysh oscillations.

where $\frac{\Delta R}{R}(E)$ is the energy dependence of the PR signal, n is the number of spectral functions to be fitted, E is the photon energy of the probe beam, E_j is the energy of the optical transition, and Γ_j, C_j and θ_j are the broadening, amplitude and phase angle, respectively. For the excitonic transition at low temperature and the band-to-band transition at room temperature, m_j is assumed to be 2 and 2.5, respectively.

Figure 5 shows low (20 K) and room (295 K) temperature PR spectra of BGaAs layers of different boron concentration together with the fitted curves (grey lines) and the moduli of PR resonances (color solid lines) obtained according to equation (2) with the parameters derived from the fit.

$$\Delta\rho_j(E) = \frac{|C_j|}{[(E - E_j)^2 + \Gamma_j{}^2]^{\frac{m_j}{2}}} \tag{2}$$

Analyzing experimental data in figure 5, first it is apparent that the optical transitions are blue-shifted with increasing boron concentration, but the observed shift is rather small for this set of samples. This phenomenon is attributed to a large band gap bowing in BGaAs as well as the strain related shift of the optical transitions. As shown in figure 1(b), BGaAs layers grown on GaP are compressively strained and this strain leads to an blue-shift of the band gap between the heavy hole (HH) band and the conduction band (HH transition). In the BGaAs samples grown on GaP, the strain-related spectral shift of HH transition expected to increase with decreasing boron concentration, as reducing the boron concentration increases the compressive strain.

We observe strong experimental evidence for strain-induced splitting in the valence band for BGaAs samples with low boron concentrations. In this case the HH transition and the optical transition between the light-hole and the conduction band (LH transition) are well resolved in PR spectra, as shown in figure 5. In addition, the optical transition between the spin–orbit split band and the conduction band (SO transition) is also clearly identifiable in these samples. With increasing boron concentration, the PR resonances related to HH, LH and SO transitions broaden, likely as a result of alloy inhomogeneities. In general, this phenomenon is expected, as alloy inhomogeneities are expected to increase with increasing boron concentration. However, the inhomogeneity-related broadening prevents clear identification of the SO and LH in the PR spectra from samples with large boron concentrations. In these cases, the PR spectra for the two samples with the largest boron concentration (15.5 and 17.7% B) were fitted with a single resonance. We note also, that fitting with a single resonance for samples with $\geqslant$10.2% B produced, within experimental uncertainty, the same energy for HH transition as the fit with two resonances. Because the intensity of HH transition is stronger than the intensity of the LH transition, the energy of HH transition can be determined unambiguously.

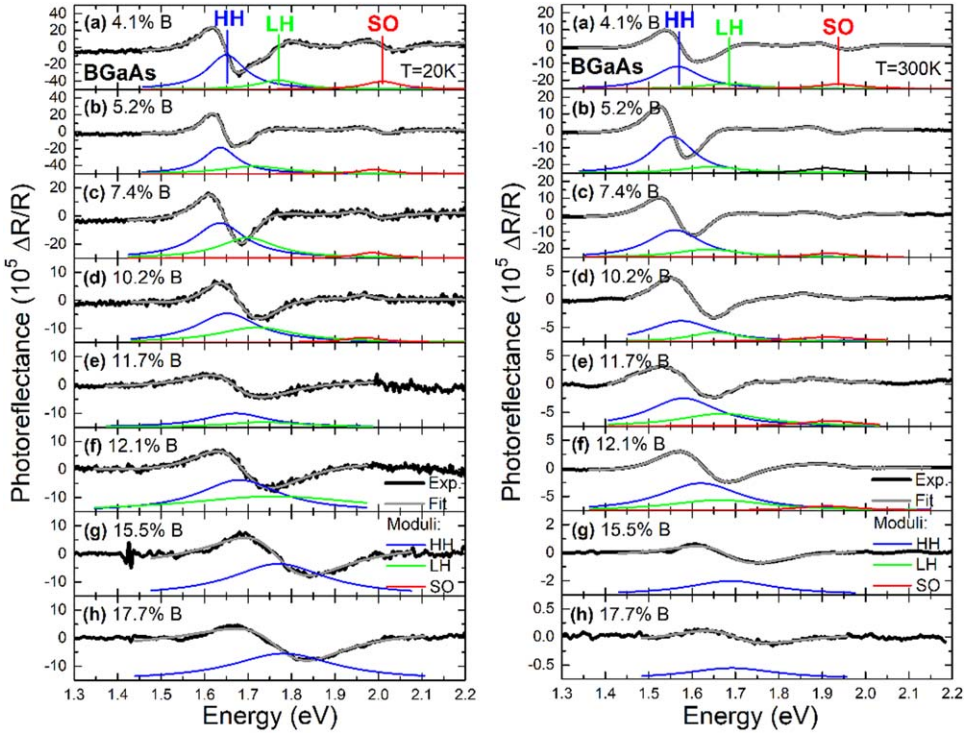

Figure 5 Low temperature (left panels) and room temperature (right panels) photoreflectance spectra of BGaAs layers of different boron concentration grown on GaP substrates. Fits to the measured spectra are shown with thick grey lines and moduli of individual optical transitions are shown with solid color lines.

In order to determine the bowing parameter for the band gap and the spin–orbit splitting, the energies of HH and SO transitions have to be shifted to values of an unstrained BGaAs layer. The strain-related shift of the HH and SO transitions can be calculated from the Bir-Pikus theory [36], where the energies of the HH, LH, and SO transitions in strained layers are given by following formulas:

$$E_{HH} = E_{HH}(\varepsilon = 0) + \delta E_H - \frac{1}{2}\delta E_U \tag{3}$$

$$E_{LH} = E_{LH}(\varepsilon = 0) + \delta E_H + \frac{1}{2}\delta E_U - \frac{1}{2}\frac{\delta E_U^2}{\Delta_{SO}} + . \tag{4}$$

$$E_{SO} = E_{SO}(\varepsilon = 0) + \delta E_H + \frac{1}{2}\delta E_U + \frac{1}{2}\frac{\delta E_U^2}{\Delta_{SO}} + ... \tag{5}$$

δE_H and δE_U are the components describing changes in the band structure related to the hydrostatic and uniaxial deformations, respectively. These components are given by expressions: $\delta E_H = a\left(\frac{C_{11}-C_{12}}{C_{11}}\right)\varepsilon_{\|}$ and $\delta E_U = 2b_{ax}\left(\frac{C_{11}+2C_{12}}{C_{11}}\right)\varepsilon_{\|}$, which depend on the in-plane strain in BGaAs layer $\varepsilon_{\|} = (a^{GaP} - a^{BGaAs})/a^{BGaAs}$. a^{GaP} is the lattice constant of GaP substrate and a^{BGaAs} is the lattice constant of BGaAs layer calculated as the linear interpolation of the lattice constant of BAs and GaAs, which are assumed to be 4.77 and 5.65 Å [37], respectively. The C_{11} and C_{12} in above formulas are the elastic constants of BGaAs which are calculated using a linear interpolation of values of $C_{11} = 122$ GPa and $C_{12} = 57$ GPa for GaAs [37] and $C_{11} = 277$ GPa and $C_{12} = 73$ GPa for BAs calculated for this purpose with the DFT methods described above. It is worth noting that the linear interpolation of elastic constants is consistent with the DFT calculations. a and b_{ax} are the hydrostatic and the uniaxial deformation potentials, respectively, which for the purpose of this correction were assumed to be the same as for GaAs.

For BGaAs layers with low B concentration where the HH and LH transitions are well resolved in PR spectra, the value of $\varepsilon_{\|}$ was determined from the splitting of HH and LH transitions and this value of $\varepsilon_{\|}$ was used to calculate the strain-related shift of HH transition and the spin–orbit splitting for the equivalent unstrained composition. In this way, the partial strain relaxation in these layers was taken into account. For BGaAs layers with higher B concentration which, the determination of $\varepsilon_{\|}$ from PR measurements is less accurate for the reasons described above. However, because these samples are coherently strained to the underlying GaP substrate, the compressive strain can be clearly determined from x-ray diffraction measurements. We then used this strain to calculate the strain-related shift of the HH transition.

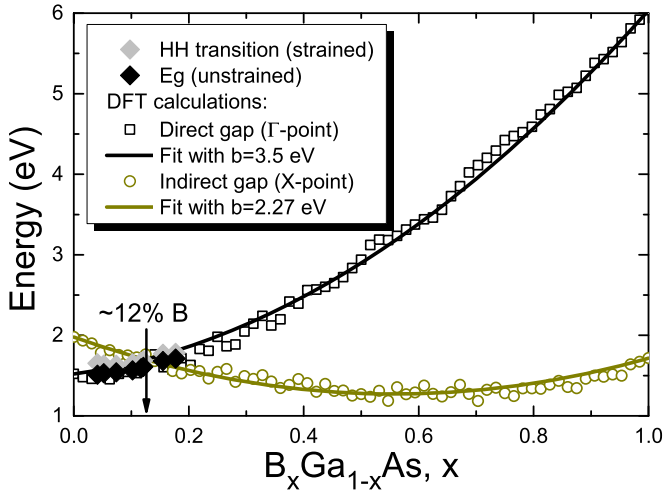

Figure 6 Energies of the HH transition (solid grey diamonds) and the unstrained band gap E_g (solid black diamonds) determined from photoreflectance measurements performed for BGaAs of different boron concentration together with energies of the direct (open squares) and the indirect (open circles) band gap determined from DFT calculations. Fitting curves of DFT data are shown by solid lines.

Figure 6 shows the energies of the HH transition (solid grey diamonds) and the unstrained band gap E_g (solid black diamonds) determined for BGaAs with various boron concentration. Additionally, the open squares and circles in figure 6 indicate the direct and indirect band gap as determined from our DFT calculations for the entire alloy compositional range. In order to determine the bowing parameter (b) for the direct and indirect gap, the calculated values were fitted using the following formula [14]

$$E_g^{BGaAs} = xE_g^{BAs} + (1-x)E_g^{GaAs} - b(1-x)x, \tag{6}$$

where E_g^{BAs} and E_g^{GaAs} is the band gap of the binary BAs and GaAs compounds, respectively. An analogous formula can be defined for the spin–orbit splitting. From the energy gap values obtained from DFT calculations, the bowing parameters for the direct and indirect gap were found to be 3.5 $\pm$ 0.1 and 2.3 $\pm$ 0.1 eV, respectively. These bowing parameters results in the crossing between direct and indirect band gaps at ~12% B in BGaAs. The bowing parameter determined for PR data was found to be 3.5 $\pm$ 0.2 eV, in excellent agreement with our DFT calculations.

Figure 7 shows the spin–orbit splitting extracted from PR measurements (solid diamonds and open diamonds) and DFT calculations (open circles). These series of data are fitted by the formula given by equation (6) where the band gap is replaced by the spin–orbit splitting. In this case b is the bowing parameter for the spin–orbit splitting. For the spin–orbit splitting, the bowing parameter determined experimentally and theoretically from DFT calculations were found to be 0.2 $\pm$ 0.1 and 0.06 $\pm$ 0.01 eV, respectively.

These consistency between the measured values (both the band gap and the spin–orbit splitting) and our theoretical calculations further highlight the strengthens of the DFT methods used in this work to determine the electronic band structure of BGaAs.

4. Conclusions

In conclusion, we present the first PR study of BGaAs alloys outside the dilute limit, Growth of BGaAs layers on GaP substrates enabled unambiguous identification of the direct optical transitions in this alloy. Using PR spectroscopy, we analyzed their energies, and determined experimentally the bowing parameters for the band gap (b_{dir} = 3.6 $\pm$ 0.2 eV) and the spin–orbit splitting (b_{SO} = 0.2 $\pm$ 0.1 eV). These experimental bowing parameters showed excellent agreement with bowing parameters extracted from DFT calculations (b_{dir} = 3.5 $\pm$ 0.1 eV). The observed agreement between theoretical and experimental values emphasize the reliability of the theoretically calculated indirect gap bowing parameter (b_{ind} = 2.3 $\pm$ 0.1 eV) and the crossing between direct and indirect gap in BGaAs at ~12% B.

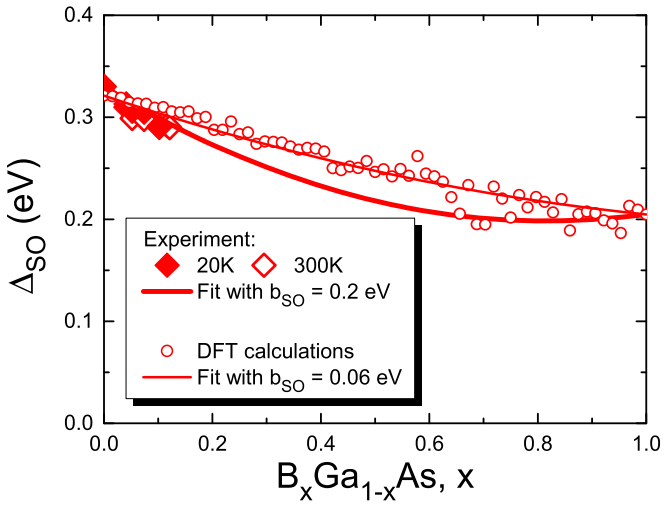

Figure 7 Energies of spin–orbit splitting determined from low (solid red diamonds) and room (open red diamonds) temperature photoreflectance measurements of BGaAs layers with different boron concentrations. Fitting curves of photoreflectance and DFT data are shown with solid lines.

Acknowledgments

This work was supported by the National Science Foundation under EECS-1933836 and EECS-1838984. J K acknowledges for the support within the Preludium grant from NCN (grant no. 2015/N/ST3/02286). The *ab initio* calculations were performed in the Wroclaw Centre for Networking and Supercomputing.

ORCID iDs

R Kudrawiec https://orcid.org/0000-0003-2593-9172
J Kopaczek https://orcid.org/0000-0003-4851-9568

References

[1] Gupta V K, Koch M W, Watkins N J, Gao Y and Wicks G W 2000 Molecular beam epitaxial growth of BGaAs ternary compounds *J. Electron. Materials* **29** 1387
[2] Geisz J F, Friedman D J, Kurtz S, Olson J M, Swartzlander A B, Reedy R C and Norman A G 2001 Epitaxial growth of BGaAs and BGaInAs by MOCVD *J. Cryst. Growth* **225** 372
[3] Shan W, Walukiewicz W, Wu J, Yu K M, Ager J W III, Li S H, Haller E E, Geisz J F, Friedman D J and Kurtz S R 2003 Band-gap bowing effects in $BxGa_{1-x}As$ alloys *J. Appl. Phys.* **93** 2696
[4] Groenert M E, Averbeck R, Hosler W, Schuster M and Riechert H 2004 Optimized growth of BGaAs by molecular beam epitaxy *J. Cryst. Growth* **264** 123
[5] Pryakhin D A, Daniltsev V M, Drozdov Yu N, Drozdov M N, Gaponova D M, Murel A V, Shashkin V I and Rushworth S 2005 Growth of BGaAs layers on GaAs substrates by metal-organic vapor-phase epitaxy *Semiconductors* **39** 11
[6] Rodriguez P, Auvray L, Dumont H, Dazord J and Monteil Y 2007 Growth and characterization of BGaAs and BInGaAs epilayers on GaAs by MOVPE *J. Cryst. Growth* **298** 81
[7] Wang Q, Ren X, Wang F, Feng J, Lv J, Zhou J, Cai S, Huang H and Huang Y 2008 LP-MOCVD growth of ternary $BxGa_{1-x}As$ epilayers on (001)GaAs substrates using TEB, TMGa and AsH3 *Microelectron. Journal* **39** 1678
[8] Ptak A J, Beaton D A and Mascarenhas A 2012 Growth of BGaAs by molecular-beam epitaxy and the effects of a bismuth surfactant *J. Cryst. Growth* **351** 122
[9] Ilahi S, Saidi F, Hamila R, Yacoubi N, Maaref H and Auvray L 2013 Shift of the gap energy and thermal conductivity in BGaAs/GaAs alloys *Physica B* **4121** 105
[10] Detz H, MacFarland D, Zederbauer T, Lancaster S, Andrews A M, Schrenk W and Strasser G 2017 Growth rate dependence of boron incorporation into BxGa1-xAs layers *J. Cryst. Growth* **477** 77
[11] Hart G L W and Zunger A 2000 Electronic structure of BAs and boride III-V alloys *Phys. Rev. B* **62** 13522
[12] Azzi S, Zaoui A and Ferhat M 2007 On the importance of the band gap bowing in Boron-based III–V ternary alloys *Solid State Commun.* **144** 245
[13] Gulyas I, Kudrawiec R and Wistey M A 2019 Electronic structure of BxGa1−xAs alloys using hybrid functionals *J. Appl. Phys.* **126** 095703
[14] Vurgaftman I, Meyer J R and Ram-Mohan L R 2001 Band parameters for III–V compound semiconductors and their alloys *J. Appl. Phys.* **89** 5815
[15] Kudrawiec R, Latkowska M, Misiewicz J, Zhuang Q, Godenir A M R and Krier A 2011 Photoreflectance study of N- and Sb-related modifications of the energy gap and spin–orbit splitting in InNAsSb alloys *Appl. Phys. Lett.* **99** 011904

[16] Kudrawiec R, Luce A V, Gladysiewicz M, Ting M, Kuang Y J, Tu C W, Dubon O D, Yu K M and Walukiewicz W 2014 Electronic band structure of GaNxPyAs1−x−y highly mismatched alloys: suitability for intermediate-band solar cells *Phys. Rev. Appl.* **1** 034007
[17] Zelazna K, Kudrawiec R, Luce A, Yu K M, Kuang Y J, Tu C W and Walukiewicz W 2018 Photoreflectance studies of optical transitions in GaNPAs intermediate band solar cell absorbers *Sol. Energy Mater. Sol. Cells* **188** 99
[18] Hohenberg P and Kohn W 1964 Inhomogeneous electron gas *Phys. Rev.* **136** B864
[19] Kohn W and Sham L J 1965 Self-consistent equations including exchange and correlation effects *Phys. Rev. 140 A1133* (https://doi.org/10.1103/PhysRev.140.A1133)
[20] Kresse G and Furthmüller J 1996 Efficiency of ab-initio total energy calculations for metals and semiconductors using a plane-wave basis set *Comp. Mater. Sci.* **6** 15
[21] Kresse G and Joubert D 1999 From ultrasoft pseudopotentials to the projector augmented-wave method *Phys. Rev. B* **59** 1758
[22] Blöchl P E 1994 Projector augmented-wave method *Phys. Rev. B* **50** 17953
[23] Zunger A, Wei S H, Ferreira L and Bernard J 1990 Special quasirandom structures *Phys. Rev. Lett.* **65** 353
[24] Van De Walle A, Tiwary P, De Jong M, Olmsted D, Asta M, Dick A, Shin D, Wang Y, Chen L Q and Liu Z K 2013 Efficient stochastic generation of special quasirandom structures *CALPHAD, Comput. Coupling Phase Diagr. Thermochem.* **42** 13
[25] Perdew J P, Burke K and Ernzerhof M 1996 Generalized Gradient Approximation Made Simple *Phys. Rev. Lett.* **77** 3865
[26] Tran F and Blaha P 2009 Accurate band gaps of semiconductors and insulators with a semilocal exchange-correlation potential *Phys. Rev. Lett.* **102** 226401
[27] Koller D, Tran F and Blaha P 2011 Merits and limits of the modified Becke-Johnson exchange potential *Phys. Rev. B* **83** 195134
[28] Camargo-Martnez J and Baquero R 2012 Performance of the modified Becke-Johnson potential for semiconductors *Phys. Rev. B* **86** 195106
[29] Monkhorst H J and Pack J D 1976 Special points for Brillouin-zone integrations *Phys. Rev. B* **13** 5188
[30] Landmann M, Rauls E, Schmidt W G, Roppischer M, Cobet C, Esser N, Schupp T, As D J, Feneberg M and Goldhahn R 2013 Transition energies and direct-indirect bandgap crossing in zinc-blende $AlxGa_{1-x}N$ *Phys. Rev. B* **87** 195210
[31] Polak M P, Scharoch P and Kudrawiec R 2017 The electronic band structure of Ge1−xSnx in the full composition range: indirect direct, and inverted gaps regimes, band offsets, and the Burstein-Moss effect *J. Phys. D* **50** 195103
[32] Popescu V and Zunger A 2010 Effective band structure of random alloys *Phys. Rev. Lett.* **104** 236403
[33] Popescu V and Zunger A 2012 Extracting E versus k-Effective band structure from super-cell calculations on alloys and impurities *Phys. Rev. B* **85** 085201
[34] Rubel O, Bokhanchuk A, Ahmed S and Assmann E 2014 Unfolding the band structure ofdisordered solids: From bound states to high-mobility Kane fermions *Phys. Rev. B* **90** 115202
[35] Aspnes D E 1973 Third-derivative modulation spectroscopy with low−field electroreflectance *Surf. Sci.* **37** 418
[36] Bir G L and Pikus G E 1976 *Symmetry and strain-induced effects in semiconductors* (New York: Wiley)
[37] DFT calculations performed within this work